


Article

Thermodynamic Analysis of the Air-Cooled Transcritical Rankine Cycle Using CO₂/R161 Mixture Based on Natural Draft Dry Cooling Towers

Yingjie Zhou ^{1,2}, Junrong Tang ³, Cheng Zhang ⁴ and Qibin Li ^{2,*} ¹ College of Computer Science, Sichuan University, Chengdu 610065, China² Key Laboratory of Low-grade Energy Utilization Technologies & Systems, Ministry of Education, College of Energy and Power Engineering, Chongqing University, Chongqing 400044, China³ College of Aerospace Engineering, Chongqing University, Chongqing 400044, China,⁴ CNNC Key Laboratory on Nuclear Reactor Thermal Hydraulics Technology, NPIC, Chengdu 610213, China

* Correspondence: qibinli@cqu.edu.cn; Tel.: +86-0185-8050-4513

Received: 6 July 2019; Accepted: 29 August 2019; Published: 29 August 2019



Abstract: Heat rejection in the hot-arid area is of concern to power cycles, especially for the transcritical Rankine cycle using CO₂ as the working fluid in harvesting the low-grade energy. Usually, water is employed as the cooling substance in Rankine cycles. In this paper, the transcritical Rankine cycle with CO₂/R161 mixture and dry air cooling systems had been proposed to be used in arid areas with water shortage. A design and rating model for mixture-air cooling process were developed based on small-scale natural draft dry cooling towers. The influence of key parameters on the system's thermodynamic performance was tested. The results suggested that the thermal efficiency of the proposed system was decreased with the increases in the turbine inlet pressure and the ambient temperature, with the given thermal power as the heat source. Additionally, the cooling performance of natural draft dry cooling tower was found to be affected by the ambient temperature and the turbine exhaust temperature.

Keywords: transcritical Rankine cycle; CO₂ mixture; R161; cooling tower; waste heat recovery

1. Introduction

The energy crisis and environmental pollution have become barriers for the sustainable development of the human society, which can be ascribed to the massive consumption of fossil fuels since the industrial revolution [1]. Scientists and technicians worldwide have employed a variety of methods to deal with these issues. Typically, harvesting the low-grade energies, such as solar energy, geothermal energy, and industrial waste heat, has been recognized as one of the effective approaches to alleviate the energy and environmental issues [2–4].

Generally, thermodynamic cycles, including the organic Rankine cycle (ORC) [5,6], Kalina cycle [7,8], and transcritical Rankine cycle (TRC) [9], which have used the low-boiling-point working fluid, are adopted to recover the low-grade energy. Of them, the TRC, which adopts the natural non-flammable and non-toxic CO₂ as the working fluid (hereinafter referred as “tCO₂”) [10–12], has more compact equipment than the Kalina cycle, and it can lead to a higher output power than ORC, thus displaying great application prospects in the field of low-grade energy utilization. However, the normal operation pressure of the tCO₂ system is about 10 MPa due to the high critical pressure of CO₂ (about 7.38 MPa), which will give rise to safety concerns. Another challenge is CO₂ condensation in the tCO₂ system as a result of the low critical temperature of CO₂ (about 304 K) [13]. It is difficult to use tCO₂ in areas with high surrounding temperature, especially, in arid areas with water shortage.

Consequently, CO₂ mixed with other fluids has been proposed as the working fluid to expand the application of tCO₂ [14]. Notably, the CO₂-based mixtures can integrate the advantages of each individual pure fluid and exhibit environmental properties as well as efficiency, which have thereby attracted increasing attention in recent years [15,16]. Furthermore, applying CO₂ mixtures in TRC can also lead to superior temperature matching with heat source over that of the CO₂ Brayton cycle. At present, the reported working fluids of CO₂ mixtures are mainly CO₂ blends with hydrocarbons, hydrofluorocarbons, and hydrofluoroolefins [17]. For instance, Dai et al. [18] investigated the thermodynamic performance of TRC using the zeotropic mixtures of CO₂ mixed with seven working fluids possessing low global warming potentials (GWP). Their results denoted that the thermal efficiency of the TRC was enhanced by the zeotropic mixtures; besides, the operation pressure of the investigated TRC was decreased. Moreover, Yang [19] examined the improvements of the economic performance of TRC with CO₂ mixtures, and discovered that, the TRC with CO₂/fluoroethane (R161) mixtures displayed better economic performance than those in other TRCs with CO₂/difluoromethane, CO₂/tetrafluoropropene, CO₂/tetrafluoroethane, CO₂/propane, and pure CO₂. Moreover, Shu et al. [20] explored the improvements in the thermodynamic and economic performance of TRC using a CO₂-based mixture to recover the engine waste heat. Their findings suggested that TRCs with CO₂/R152a, CO₂/R161, and CO₂/R32 mixtures could achieve the optimal performances, along with a low operation pressure and the optimal total heat transfer area. Thus, TRC with CO₂/R161 mixture is promising to be used to recover the low-grade energy.

The CO₂/R161 mixture is associated with the superiorities of fine thermostability, as well as optimal thermodynamic and economic performances in TRC, which can thereby be utilized for low-grade energy recovery at a high ambient temperature. Nonetheless, few existing studies [13–20] have examined the cooling process of TRC with CO₂/R161 mixture. Usually, water cooling is employed for analysis, but the water resource issue [21] has drawn growing attention, since water is a kind of valuable natural resource. On this account, the direct air cooling technique will be an ideal approach for thermodynamic cycles in arid areas with water shortage.

Consequently, the TRC using CO₂/R161 mixture with the direct air cooling system had been proposed and investigated in this paper. Firstly, the thermodynamic model of the TRC system was constructed and verified. Subsequently, the natural draft dry cooling tower (NDDCT) model was established based on the experimental data from Li et al. [22]. Afterward, the performance of the NDDCT was analyzed under different ambient temperatures and thermal loads of turbine exhaust. Moreover, this work was expected to shed valuable light on the mixture working fluids [23–25] and ORC using the direct air cooling system [26].

2. Model and Considerations

The schematic diagram of the power plant is presented in Figure 1. As can be observed, the power plant consisted of four basic components, including the heater, the turbine, the cooling tower, and the pump. Moreover, there were four processes regarding the thermodynamic cycle of the working fluid in the system, among which, in process 1–2, the condensed fluid was pumped into the high pressure state; in process 2–3, the working fluid experienced phase transition and changed into the high temperature and high pressure supercritical state in the heater; in process 3–4, the supercritical fluid was expanded to produce power in the turbine; and in process 4–1, the working fluid was cooled in the cooling tower. Here, the NDDCT was selected as the condenser, which could cool the working fluid with no water loss and almost no parasitic power consumption [27].

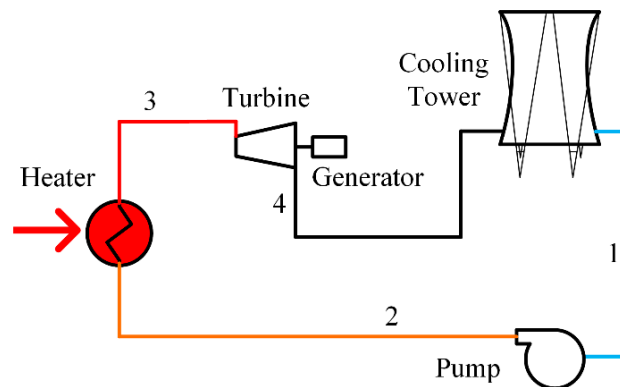


Figure 1. Schematic diagram of the power plant.

Additionally, the temperature–entropy (T – s) diagram of the corresponding power plant system using $\text{CO}_2/\text{R161}$ (50/50 wt.%) is plotted in Figure 2. Noteworthy, the working fluid had experienced the single- and two-phase condensation processes in the NDDCT, during which temperature glide had occurred.

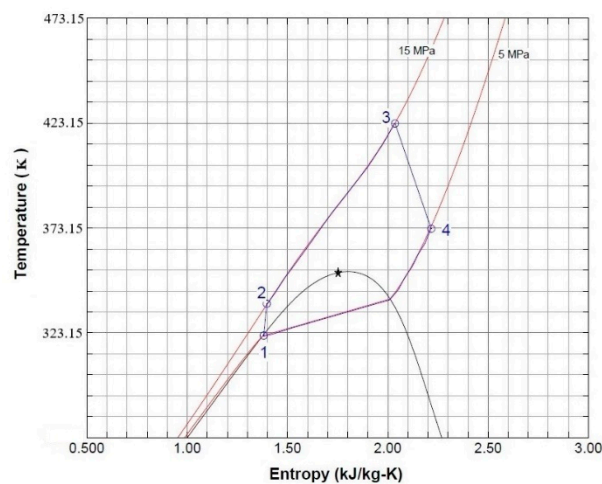


Figure 2. Temperature–entropy (T – s) diagram ($\text{CO}_2/\text{R161}$: 50/50 wt.%) of the transcritical Rankine cycle (TRC).

Figure 3 presents the critical pressure and critical temperature for the $\text{CO}_2/\text{R161}$ mixtures with various mass fractions [28]. Clearly, the critical temperature of the mixtures was increased with the increase in the mass fraction of R161. Meanwhile, the critical pressure of the mixtures was decreased, which rendered a lower TRC operation pressure than that of tCO_2 , and laid the foundation for the practical application of TRC using CO_2 mixtures.

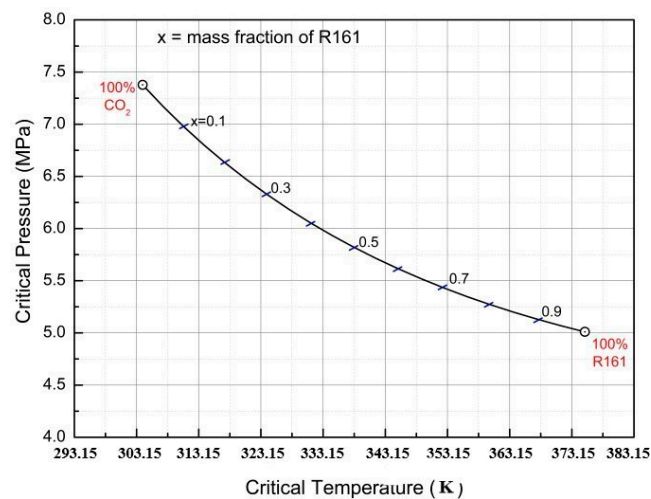


Figure 3. The critical pressure and critical temperature for CO₂/R161 mixtures.

2.1. Calculation Assumptions

The assumptions of the power plant system are exhibited in Table 1. Typically, the heat source of the system could be solar energy, geothermal energy, or waste heat. Therefore, the thermal power of 500.00 kW was given as the heat source for the universality of the system, while the range of the turbine inlet temperature was 423.15–473.15 K. In addition, the mass flow of the working fluid was calculated according to the heat balance equation. The annual average air temperature was 298.15 K, and, in this paper, the air temperature fluctuated within the range of 293.15–303.15 K. Furthermore, there was no pressure loss in the pipeline and heat exchanger, and the whole power plant system operated at the steady state.

Table 1. Design operation parameters.

Parameter	Value
Thermal power of heat source (kW)	500.00
Annual average air temperature (K)	298.15
Isentropic turbine efficiency	0.70
Isentropic pump efficiency	0.80
Turbine inlet temperature (K)	423.15
Turbine inlet pressure (MPa)	15.00
Pressure losses	0.00

2.2. Mathematical Model

The equations for the system components were based on the first law of thermodynamics. The National Institute of Standards and Technology (NIST) REFPROP program [29] was used for physical properties of CO₂/R161 mixture.

As for the turbine:

$$W_t = \text{mass} \cdot (h_3 - h_4). \quad (1)$$

For the pump:

$$W_p = \text{mass} \cdot (h_2 - h_1). \quad (2)$$

For the heater:

$$Q_{in} = \text{mass} \cdot (h_3 - h_2). \quad (3)$$

For cooling tower:

$$Q_{cool} = \text{mass} \cdot (h_4 - h_1). \quad (4)$$

The heat exchanger in the cooling tower was made up of bundles with the same structural and functional characteristics. It can be seen in Figure 4 that each bundle was composed of 10 finned tubes arranged in five rows. Meanwhile, the working fluid would enter the bundle through the left side of the fifth row in the finned tubes and leave the bundle at the right side of the first row in the finned tubes. Then, the air would cool the working fluid by flowing from the bottom to the top of the bundle. The calculation for the heat exchanger model is also presented in Figure 4. Generally, the traditional method of heat exchanger modeling is only valid for a working fluid with constant properties. In this study, the nodal approach was adopted in designing the heat exchanger, in which each row of the heat exchanger bundles was divided into 24 sections, as if a number of small heat exchangers were connected in series.

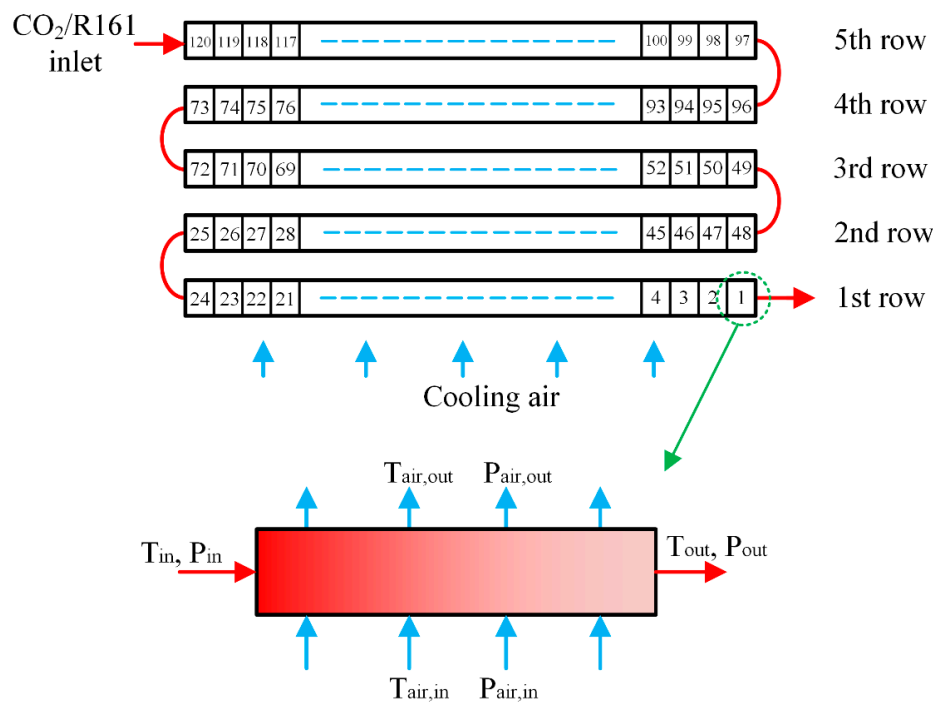


Figure 4. Heat exchanger bundles and nodal approach for the heat exchanger model.

The heat balance equation between CO₂ mixture and air was as follows,

$$Q_{ct} = m_{CO_2} \cdot (h_{CO_2,i} - h_{CO_2,o}) = m_{air} \cdot c_{p,air} \cdot (T_{air,i} - T_{air,o}), \quad (5)$$

where Q_{ct} is the heat emission of the cooling tower (W), h_{CO_2} represents the enthalpy of CO₂ (J·kg⁻¹), while i and o stand for the inlet and outlet of the working fluid, respectively, and $c_{p,air}$ indicates the average heat capacity of air (J·kg⁻¹·K⁻¹).

Additionally, the product of the heat transfer area and the overall heat transfer coefficient (UA) of the heat exchanger could be obtained through the logarithmic mean temperature difference (LMTD), as displayed below.

$$Q = U \cdot A \cdot F_T \cdot \Delta T_{LMTD}, \quad (6)$$

where U is the thermal conductivity of the system (W·m⁻²·K⁻¹), A stands for the area of heat transfer (m²), F_T indicates the correction factor of LMTD (which amends the counter current flow as the cross-flow), and ΔT_{LMTD} represents the logarithmic mean temperature (K), which can be calculated as follows,

$$\Delta T_{LMTD} = (\Delta T_1 - \Delta T_2) / \ln(\Delta T_1 / \Delta T_2) \quad (7)$$

when the working fluid experienced counter current flow in the heat exchanger, $\Delta T_1 = T_{\text{CO}_2,o} - T_{\text{air},i}$, $\Delta T_2 = T_{\text{CO}_2,i} - T_{\text{air},o}$.

On the other hand, the condenser could be divided into the superheated single-phase region and the two-phase region based on the working fluid state at the turbine outlet. For the single-phase region of the CO_2 mixture, the Krasnoshchekov–Petukhov correlation [30,31] was employed,

$$Nu_0 = \frac{(f/8)Re_D Pr}{1.07 + 12.7(f/8)^{1/2}(Pr^{2/3} - 1)}, \quad (8)$$

$$U = \frac{k}{D} Nu_0 \left(\frac{\mu_b}{\mu_w} \right)^{0.11} \left(\frac{k_b}{k_w} \right)^{-0.33} \left(\frac{c_p}{c_{pb}} \right)^{0.35}, \quad (9)$$

$$f = (0.790 \ln Re_D - 1.64)^{-2}, \quad (10)$$

where U represents the heat transfer coefficient and D suggests the inner diameter of the tube.

The following correlation [32] was used for the two-phase region of the CO_2 mixture.

$$Nu = 0.729 \left[\frac{g \rho_f (\rho_f - \rho_g) D \delta^3 i'_{fg}}{\mu_f k_r (T_{\text{sat}} - T_{\text{wall}})} \right]^{1/4}, \quad (11)$$

where g represents acceleration due to gravity, ρ_f and ρ_g are the densities of liquid and vapor working fluid, and i'_{fg} is the modified latent heat of vaporization.

The heat transfer coefficient at the air side [22] was calculated as follows,

$$h_a A_a = 0.0143 Re_a^2 + 83.2 Re_a + 22210, \quad (12)$$

where h_a is the air side heat transfer coefficient, A_a stands for the air side heat transfer area, and Re_a indicates the Reynolds number of air. Moreover, the characteristic length of Re_a was deemed as the equivalent circular diameter of the air flow passage, which was 1.7×10^{-2} m for this particular heat exchanger.

The structure chart of the NDDCT and the distribution diagram of air side resistance are displayed in Figures 5 and 6, respectively. Clearly, the NDDCT consisted of the tower support columns, the heat exchanger bundles, the hyperbolic-type tower shell, and the sensors.

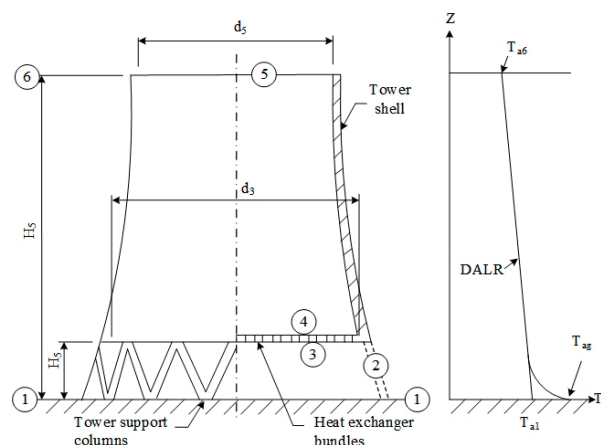


Figure 5. The distribution of heat exchangers in natural draft dry cooling tower (NDDCT). *DALR: Dry adiabatic lapse rate.

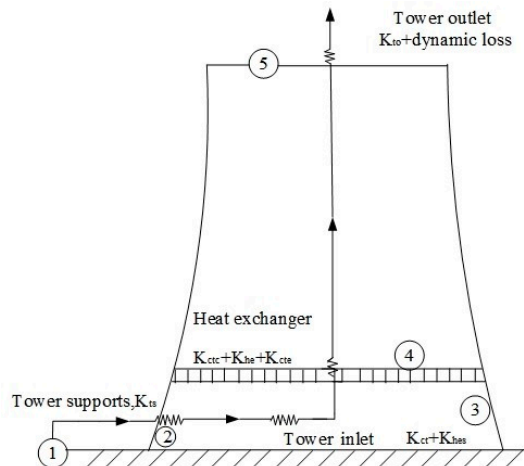


Figure 6. The coefficients of losses of air in NDDCT.

The ventilation equation represents the balance equation between the buoyancy with the result of air heating and the air pressure loss in the NDDCT, as shown below:

$$\begin{aligned}
 & p_{a1} \left[\left\{ 1 - 0.00975(H_3 + H_4) / (2T_{a1}) \right\} \right]^{3.5} \\
 & \times \left\{ 1 - 0.00975(H_5 - H_3/2 - H_4/2) / T_{a4} \right\}^{3.5} \\
 & - (1 - 0.00975H_5 / T_{a1})^{3.5} \\
 & = (K_{ts} + K_{ct} + K_{hes} + K_{ctc} + K_{he} + K_{cte})_{he} (m_a / A_{fr})^2 / (2\rho_{a34}) \\
 & \times \left[1 - 0.00975(H_5 - H_3/2 - H_4/2) / T_{a4} \right]^{3.5} \\
 & + (1 + K_{to}) (m_a / A_5)^2 (2\rho_{a5})
 \end{aligned} \quad (13)$$

where p_{a1} is the air pressure at state 1 in Figure 1 (Pa), T_{a1} suggests the air temperature at state 1 (K), H_3 represents the distance between the heat exchanger bundles bottom and the ground (m), H_4 indicates the distance between the top of the heat exchanger bundles and the ground (m), H_5 is the distance between the tower outlet and the ground (m), T_{a4} stands for the air temperature at state 4 (K), m_a is indicative of the air flow ($\text{kg}\cdot\text{s}^{-1}$), A_{fr} is the face area of the heat exchanger bundle bottom (m^2), ρ_{a34} signifies the average air density of the heat exchanger bundles ($\text{kg}\cdot\text{m}^{-3}$), A_5 denotes the outlet area of the cooling tower (m^2), ρ_{a5} represents the outlet air density of cooling tower ($\text{kg}\cdot\text{m}^{-3}$), and K indicates the coefficients of air loss in the NDDCT. More details are presented in Table 2.

Table 2. The coefficients of loss of air in NDDCT [33].

Loss Coefficient	Equation
The tower support loss coefficient, K_{ts}	$K_{ts} = \frac{2\Delta p_{ats}\rho_{a34}}{(\frac{m_a}{A_{fr}})^2} = \frac{C_{Dts}L_{ts}d_{ts}n_{ts}A_{fr}^2}{(\pi d_3 H_3)^3} \left(\frac{\rho_{a34}}{\rho_{a1}} \right)$
Contraction loss coefficient, K_{ctc}	$K_{ctc} = \left(1 - \frac{2}{\sigma_c} + \frac{1}{\sigma_c^2} \right) \left(\frac{\rho_{a34}}{\rho_{a1}} \right) \left(\frac{A_{fr}}{A_{e3}} \right)^2$
Expansion loss coefficient, K_{cte}	$K_{cte} = \left(1 - \frac{A_{e3}}{A_3} \right)^2 \left(\frac{\rho_{a34}}{\rho_{a1}} \right) \left(\frac{A_{fr}}{A_{e3}} \right)^2$
Cooling tower inlet loss coefficient, K_{ct}	$K_{ct} = K_{cthe} (\rho_{a34} / \rho_{a1}) (A_{fr} / A_{e3})^2$ Terblanche and Kroger correlation $K_{cthe} = [100 - 18(\frac{d_3}{H_3}) + 0.94(\frac{d_3}{H_3})^2] \chi K_{he}^{[-1.28 + 0.183(\frac{d_3}{H_3}) - 7.769 \times 10^{-3}(\frac{d_3}{H_3})^2]}$
Cooling tower outlet loss coefficient, K_{to}	$K_{to} = \frac{\Delta p_{a56}}{\frac{\rho_{a5} v_{a5}^2}{2}} = \frac{2\rho_{a5}\Delta p_{a56}}{(\frac{m_a}{A_5})^2} = -0.28Fr_D^{-1} + 0.04Fr_D^{-1.5}$ $Fr_D = (\frac{m_a}{A_5})^2 / [\rho_{a5}(\rho_{a6} - \rho_{a5})gd_5]s$
Heat exchanger loss coefficient, K_{he}	Characteristic Reynolds number, $Ry = \frac{m_a}{\mu_{a34}A_{fr}T}$ $K_{he} = 31383.8475Ry^{-0.332458} + \frac{2}{\sigma_a^2} \left(\frac{\rho_{a3} - \rho_{a4}}{\rho_{a3} + \rho_{a4}} \right)$

The specified parameters for the design of the NDDCT are listed in Table 3. The design flow of the NDDCT was built on the parameter iteration according to the energy conservation equation and

the ventilation equation. Typically, the minimum ΔT_{LMTD} was 5.00 K. The detailed data for the heat exchanger are listed in Table 4.

Table 3. Specified parameters for the design of the NDDCT.

Parameter	Unit	Value
Aspect ratio of cooling tower, H_5/d_3	-	1.40
Tower inlet height, H_3	m	5.00
Tower diameter ratio, d_5/d_3	-	0.70
Heat exchanger coverage of tower inlet, A_{fi}/A_3	-	0.65
Number of tower supports, n_{ts}	-	$d_3/(82.96/60)$
Length of tower support, L_{ts}	m	$H_3 \times (15.78/13.67)$

Table 4. The detailed data for the heat exchanger.

Heat Exchanger Parameter	Unit	Value
Hydraulic diameter of tube	m	9.00×10^{-3}
Inside area of tube per unit length	m ²	2.85×10^{-2}
Inside cross-sectional flow area	m ²	6.40×10^{-5}
Length of finned tube	m	3.84
Effective length of tube	m	3.79
Number of tube rows	-	5
Number of tubes per bundles	-	220
Number of water passes	-	10
Number of bundles	-	18
Total effective frontal area	m ²	76.60
Fin root diameter	m	9.50×10^{-3}
Fin pitch	m	2.10×10^{-3}

3. Results and Discussion

3.1. Thermodynamic Analysis

Firstly, the calculated thermal efficiency of CO₂/R161 TRC was compared with that of Dai et al. [18]. As shown in Figure 7, the simulation results were consistent with those previously reported, which verified the correctness of our calculation. Moreover, those results also suggested that the thermal efficiency of CO₂/R161 TRC was enhanced with the decrease in the CO₂ mass fraction in CO₂/R161 mixtures.

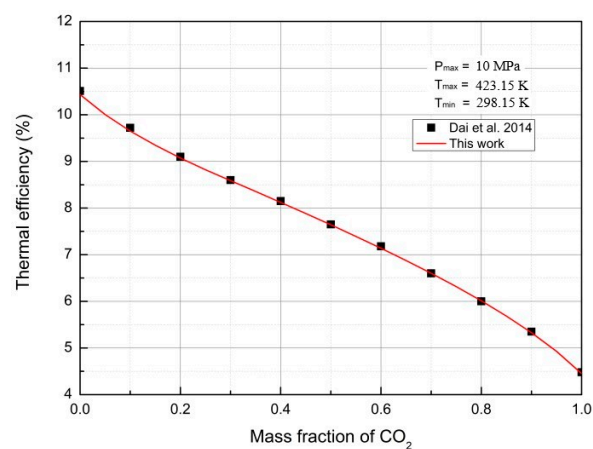


Figure 7. Thermal efficiencies for CO₂/R161 TRC.

On the other hand, Figure 8 plots the changes in thermal efficiency depending on the variation of turbine inlet pressure at various turbine inlet temperatures using CO₂/R161 (mass fraction of 0.5/0.5). As can be observed, the thermal efficiency was first increased and then decreased as the turbine inlet pressure was elevated. In other words, there was an optimal turbine inlet pressure to obtain the maximal thermal efficiency of the system. In addition, the optimal turbine inlet pressure was boosted with the increase in turbine inlet temperature. In our study, the optimal turbine inlet pressure was determined to be about 8.00 MPa at the turbine inlet temperature of 373.15 K, which was changed to about 18.00 MPa at the turbine inlet temperature of 473.15 K.

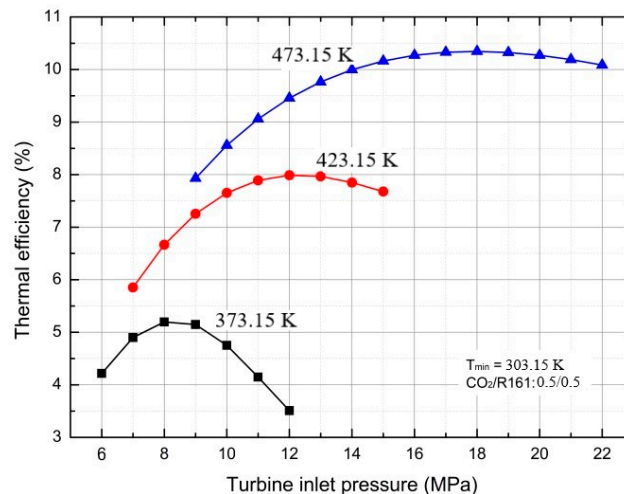


Figure 8. The relationships between thermal efficiency and turbine inlet pressure under various turbine inlet temperatures.

The evolution of the thermal efficiency with the variations in mass fraction and turbine inlet pressure at different minimum circulation temperatures is exhibited in Figure 9. Obviously, the thermal efficiency increased with the increase in turbine inlet pressure in the presence of low R161 mass fraction. In the meantime, the maximum thermal efficiency appear as the R161 mass fraction was increased. However, the thermal efficiency was gradually decreased with the increase in turbine inlet pressure at the high R161 mass fraction. Besides, the minimum circulation temperature would also affect the thermal efficiency of the system.

Table 5 lists the optimal operation parameters of CO₂/R161 TRC at the condensing temperature of 308.15 K and the turbine inlet temperature of 423.15 K. As can be seen, the optimal thermal efficiency was about 7.40%, the optimal output work was about 37.00 kW, the optimal working medium flow was 1.60 kg/s, and the heat rejection of the condenser was about 463.00 kW.

Table 5. Design conditions for the air-cooled CO₂/R161 TRC.

Plant Solution	Value
Turbine inlet temperature (K)	423.15
Turbine inlet pressure (MPa)	12.45
Cycle efficiency (%)	7.42
Plant power output (kW)	37.11
Condensing temperature (K)	308.15
CO ₂ /R161 mass fraction ratio	0.5/0.5
Vapor fraction at turbine outlet (%)	100.00
Turbine outlet temperature (K)	345.00
Mass flow rate of the working fluid (kg·s ⁻¹)	1.62
Heat rejection (kW)	462.89

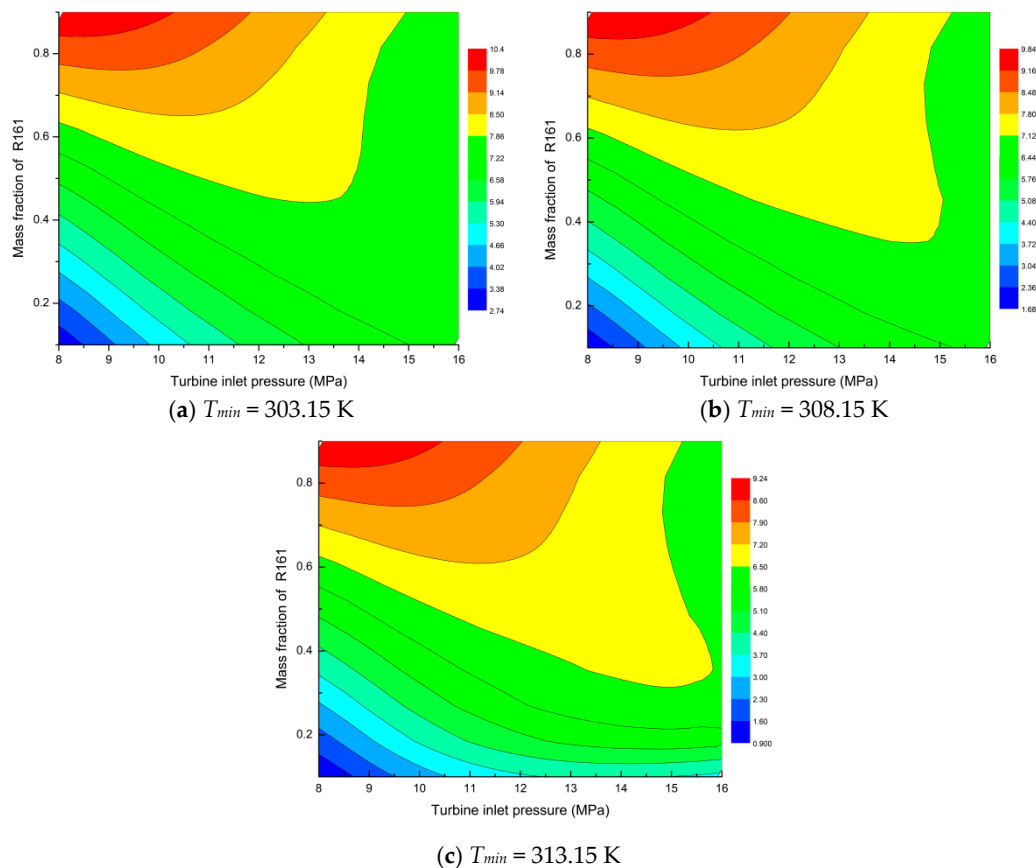


Figure 9. Contours of thermal efficiency with variation of mass fraction and turbine inlet pressure at different circulation minimum temperatures.

3.2. Design Parameters and Performance Analysis of Cooling Tower

Notably, the as-prepared TRC with CO₂ blends was more sensitive to the environment temperature, since the CO₂ mixtures could directly exchange heat with air in the NDDCT, which was different from the conventional indirect cooling system. Therefore, the effects of the environment temperature and temperature variation of CO₂ mixtures on the system were also investigated.

The design parameters of the NDDCT at the condenser heat rejection of about 463.00 kW (as discussed in Table 5) are listed in Table 6. As can be seen, the height of the cooling tower was 10.00 m; the diameters of the inlet and the outlet of the cooling tower were 7.14 and 5 m, respectively; the number of heat exchanger bundles was seven; the working fluid outlet temperature was 307.98 K; and the air mean outlet temperature was about 318.85 K.

The temperature profiles of CO₂ mixture and air in the cooling tower are presented in Figure 10. As can be figured out, the CO₂ mixture had experienced transition from the single-phase vapor state to the vapor–liquid two-phase state in the fifth row of the finned tubes. Afterward, the CO₂ mixture was slowly condensed into the saturated liquid during cooling from the fourth to the first row of the finned tubes. It is noted that the air temperature was plotted between every layer of finned tubes in the air-cooled heat exchangers. The discontinuity in the air temperature trends during phase change of the CO₂/R161 mixture is due to an abrupt decrease in mixture heat transfer coefficient, which results in a high temperature difference in the vapor phase. However, the smaller rejection heat in the vapor phase reduced the air temperature difference. Moreover, the air temperature through the overall length of the cooling tower is shown in Appendix A Figure A1. The heat transfer coefficient of CO₂ mixture variation in the heat exchanger is presented in Figure 11. Clearly, the heat transfer coefficient of the CO₂ mixture was about 200 W/m²·K at the single-phase vapor state, while that was increased to

3000 W/m²·K at the vapor–liquid two-phase state. The temperature difference in each row was about 3.00 K, and the outlet temperature of air at the fifth row of the finned tubes was about 318.15–320.15 K.

Table 6. The design parameters of the NDDCT at the condenser heat rejection of about 463 kW.

Parameters	Cooling Tower System
Tower height (m)	10.00
Tower outlet diameter (m)	5.00
Tower inlet diameter (m)	7.14
Tower inlet height (m)	4.00
Number of heat exchanger bundles	7
Frontal area (m ²)	29.80
Working fluid inlet temperature (K)	345.00
Working fluid outlet temperature (K)	307.98
Working fluid inlet pressure (MPa)	3.89
Working fluid mass flow (kg·s ^{−1})	1.62
Heat rejection (kW)	463.00
Air mass flow (kg·s ^{−1})	22.20
Air mean outlet temperature (K)	318.85

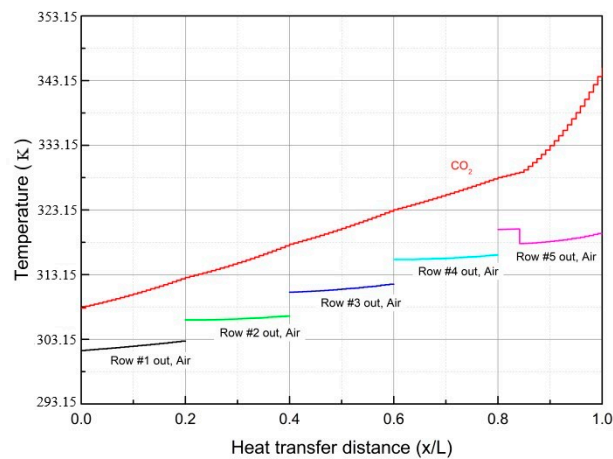


Figure 10. Temperature profile in the cooling tower.

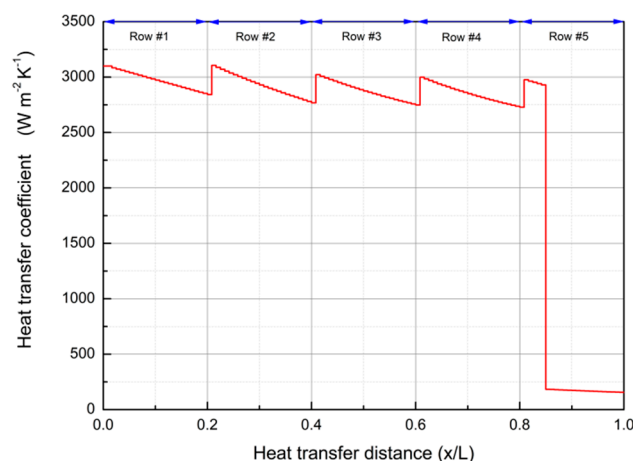


Figure 11. Heat transfer coefficient of CO₂ mixture variation in the heat exchanger.

The air velocity through the heat exchanger bundles is calculated and presented in Figure 12. It is noted that the discontinuity in the air velocity trend is due to data selection, which are ones between every layer of finned tubes. Actually, air flows across tubes with a continuous velocity. The air velocity through the overall length of the cooling tower is shown in Appendix A Figure A2. As can be seen, the

air velocity was about 0.63 m/s at the first row of finned tubes, which was increased to 0.67 m/s at the fifth row of finned tubes. This was because air heating would result in a decrease in density and an increase in buoyancy, thus, giving rise to the increased air velocity through the heat exchanger bundles.

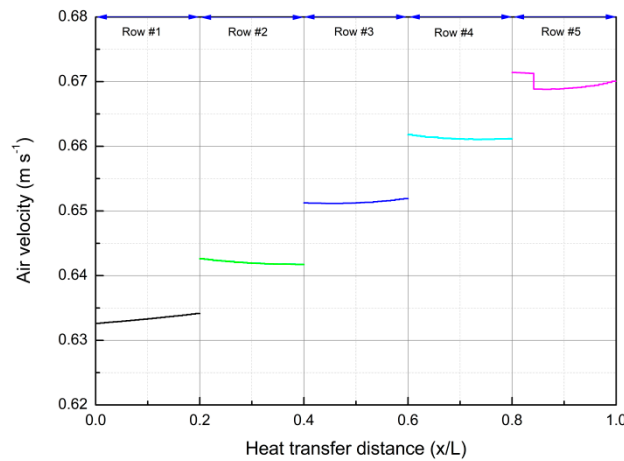


Figure 12. The air velocities through the heat exchanger bundles.

The effects of ambient temperature on the CO₂ outlet temperature in the condenser, the heat rejection of cooling tower, and the mass flow rate of air through the cooling tower are calculated, as presented in Figures 13–15, respectively. Specifically, the increase in ambient temperature would reduce the mass flow rate of air and decrease the heat rejection of the NDDCT, thus, deteriorating the cooling of CO₂ mixtures. For instance, the turbine exhaust temperature of the CO₂ mixture was 345.00 K, the heat rejection of the cooling tower was 450.00 kW, and the outlet temperature of CO₂ in the condenser was 312.15 K at the ambient temperature of 303.15 K. Importantly, the performance of the NDDCT was enhanced with the increases in ambient temperature and the heat rejection of cooling tower coupled with the decrease in CO₂ outlet temperature in the condenser. Noteworthy, the pressure of the CO₂ mixture was changed with the alteration in the condensation temperature of CO₂ mixture.

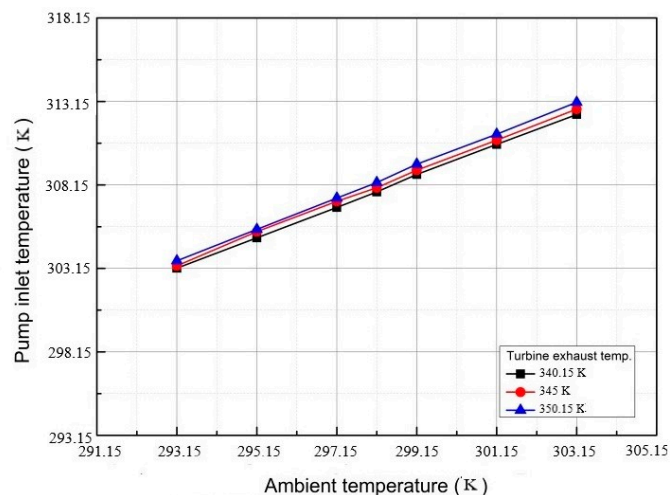


Figure 13. Outlet temperature of CO₂ in the condenser at different ambient temperatures.

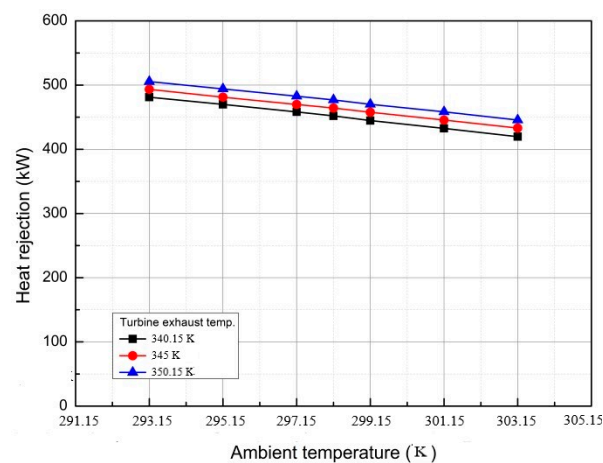


Figure 14. Influence of ambient temperature on heat rejection of cooling tower.

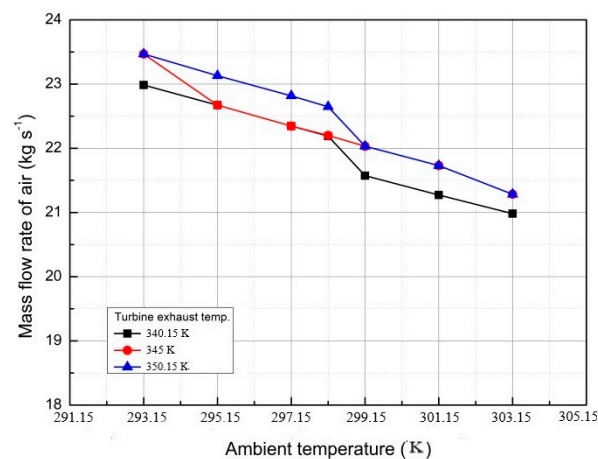


Figure 15. Mass flow rate of air through the cooling tower at different ambient temperatures.

In addition, as presented in Figure 14, the heat rejection of cooling tower was increased as the turbine exhaust temperature was elevated (Figure 13) at the same ambient temperature, while the CO₂ outlet temperature in the condenser remained largely unchanged. Typically, the driving force of air flow in the NDDCT was the density difference between the hot air in the cooling tower and the cool air out of the cooling tower. Additionally, the heat exchange was driven by the temperature difference between the air and the CO₂ mixture. Thus, the density difference between air in and out of the cooling tower was enlarged as the turbine exhaust temperature was elevated, which would result in the increased mass flow rate of air and air velocity, finally boosting the heat rejection of the cooling tower.

4. Conclusions

A transcritical Rankine cycle system with natural draft dry cooling tower using CO₂/R161 blends has been established in this paper. The thermodynamic performance and optimal operation parameters of the system, together with the cooling performance of natural draft dry cooling tower, are discussed. In addition, the design procedures of the natural draft dry cooling tower in a transcritical Rankine cycle using a CO₂/R161 mixture are provided. The conclusions can be drawn that the CO₂/R161 mixture has the potential to be used in arid areas, using dry air cooling methods with great thermodynamic performance. The decrease in ambient temperature will lead to the increase in the mass flow rate of air and the heat rejection of cooling tower, which will result in the lower inlet temperature of CO₂/mixture in the pump. Moreover, the thermal efficiency of transcritical Rankine cycle using

CO₂/R161 is decreased with increases in the turbine inlet pressure and ambient temperature, with thermal power being used as the heat source.

Author Contributions: Conceptualization, C.Z. and Q.L.; methodology, Y.Z., J.T., and C.Z.; software, Y.Z.; validation, J.T.; writing—original draft preparation, Y.Z., J.T., C.Z., and Q.L.; writing—review and editing, Y.Z., J.T., C.Z., and Q.L.; project administration, Q.L.; funding acquisition, Q.L.

Funding: This work is supported by the National Natural Science Foundation of China (no. 51876015) and Fundamental Research Funds for the Central Universities (no. 2018CDXYDL0001).

Acknowledgments: The authors would like to acknowledge their colleagues from the Key Laboratory of Low-Grade Energy Utilization Technologies and Systems, Ministry of Education for their perspectives and suggestions related to data collection and statistical analysis.

Conflicts of Interest: The authors declare no conflict of interest.

Nomenclature

h	enthalpy (kJ/kg)
Q	heat transfer rate (kW)
m	mass flow rate (kg/s)
U	heat transfer coefficient ($\text{W}\cdot\text{m}^{-2}\cdot\text{K}^{-1}$)
c_p	specific heat capacity (kJ/kg·K)
T	temperature (K)
A	heat exchanger area (m^2)
D	inner diameter (m)
K	coefficient of loss of air
H	height (m)
L	length (m)

Greek symbols

ΔT	temperature difference (K)
ρ	density (kg/m^3)

Acronyms

ORC	organic Rankine cycle
TRC	transcritical Rankine cycle
LMTD	logarithmic mean temperature difference
NDDCT	natural draft dry cooling tower

Subscripts

p	pump
t	turbine
$cool$	cool water
a	air
i	inlet
o	outlet

Appendix A

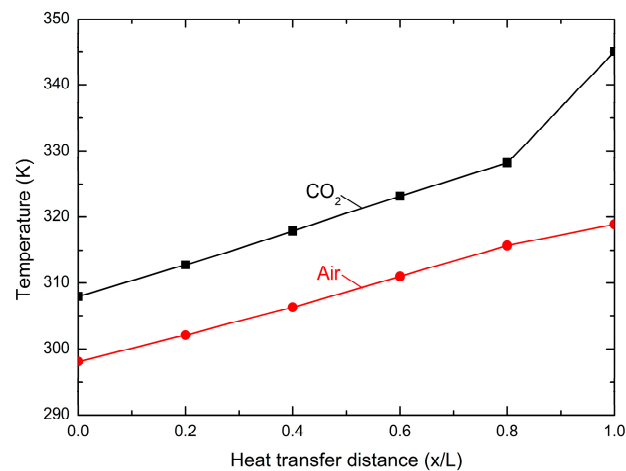


Figure A1. The air temperature through the overall length of the cooling tower.

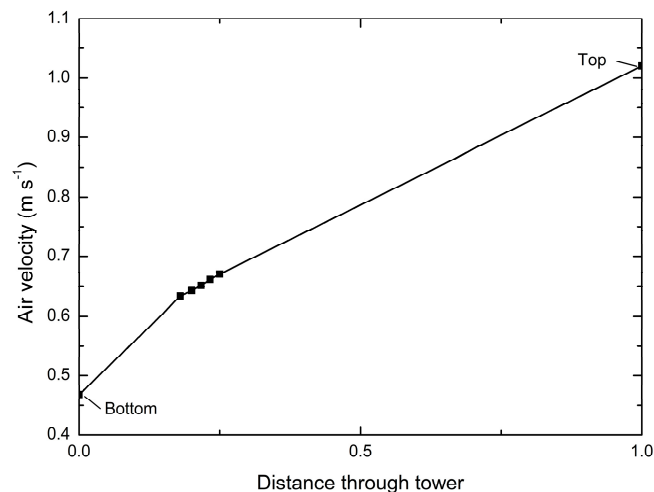


Figure A2. The air velocity through the overall length of the cooling tower.

References

1. Vélez, F.; Segovia, J.J.; Martín, M.C.; Antolín, G.; Chejne, F.; Quijano, A. A technical, economical and market review of organic Rankine cycles for the conversion of low-grade heat for power generation. *Renew. Sustain. Energy Rev.* **2012**, *16*, 4175–4189.
2. Yamamoto, T.; Furuhashi, T.; Arai, N.; Mori, K. Design and testing of the Organic Rankine Cycle. *Energy* **2001**, *26*, 239–251. [[CrossRef](#)]
3. Wang, S.; Liu, C.; Zhang, C.; Xu, X.; Li, Q. Thermo-economic evaluations of dual pressure organic Rankine cycle (DPORC) driven by geothermal heat source. *J. Renew. Sustain. Energy* **2018**, *10*, 063901. [[CrossRef](#)]
4. Ding, Y.; Liu, C.; Zhang, C.; Xu, X.; Li, Q.; Mao, L. Exergoenvironmental model of Organic Rankine Cycle system including the manufacture and leakage of working fluid. *Energy* **2018**, *145*, 52–64. [[CrossRef](#)]
5. Zhang, C.; Liu, C.; Xu, X.; Li, Q.; Wang, S.; Chen, X. Effects of superheat and internal heat exchanger on thermo-economic performance of organic Rankine cycle based on fluid type and heat sources. *Energy* **2018**, *159*, 482–495. [[CrossRef](#)]
6. Gao, H.; Liu, C.; He, C.; Xu, X.; Wu, S.; Li, Y. Performance analysis and working fluid selection of a supercritical Organic Rankine Cycle for low grade waste heat recovery. *Energies* **2012**, *5*, 3233–3247. [[CrossRef](#)]
7. Marston, C.H. Parametric analysis of the Kalina cycle. *J. Eng. Gas Turb. Power* **1990**, *112*, 107–116. [[CrossRef](#)]

8. Gao, H.; Chen, F. Thermo-economic analysis of a bottoming Kalina cycle for internal combustion engine exhaust heat recovery. *Energies* **2018**, *11*, 3044. [[CrossRef](#)]
9. Zhang, C.; Liu, C.; Xu, X.; Li, Q.; Wang, S. Energetic, exergetic, economic and environmental (4E) analysis and multi-factor evaluation method of low GWP fluids in trans-critical organic Rankine cycles. *Energy* **2019**, *168*, 332–345. [[CrossRef](#)]
10. Sadreddini, A.; Ashjari, M.A.; Fani, M.; Mohammadi, A. Thermodynamic analysis of a new cascade ORC and transcritical CO₂ cycle to recover energy from medium temperature heat source and liquefied natural gas. *Energy Convers. Manag.* **2018**, *167*, 9–20. [[CrossRef](#)]
11. Rony, R.U.; Yang, H.; Krishnan, S.; Song, J. Recent advances in transcritical CO₂ (R744) heat pump system: A review. *Energies* **2019**, *12*, 457. [[CrossRef](#)]
12. Omar, A.; Saghafifar, M.; Mohammadi, K.; Alashkar, A.; Gadalla, M. A review of unconventional bottoming cycles for waste heat recovery: Part II—Applications. *Energy Convers. Manag.* **2019**, *180*, 559–583. [[CrossRef](#)]
13. Yari, M.; Mahmoudi, S.M.S. Thermodynamic analysis and optimization of novel ejector-expansion TRCC (transcritical CO₂) cascade refrigeration cycles (Novel transcritical CO₂ cycle). *Energy* **2011**, *36*, 6839–6850. [[CrossRef](#)]
14. Xia, J.; Wang, J.; Zhang, G.; Lou, J.; Zhao, P.; Dai, Y. Thermo-economic analysis and comparative study of transcritical power cycles using CO₂-based mixtures as working fluids. *Appl. Therm. Eng.* **2018**, *144*, 31–44. [[CrossRef](#)]
15. Guo, J.; Li, M.; Xu, J.; Yan, J.; Wang, K. Thermodynamic performance analysis of different supercritical Brayton cycles using CO₂-based binary mixtures in the molten salt solar power tower systems. *Energy* **2019**, *173*, 785–798. [[CrossRef](#)]
16. Manzolini, G.; Binotti, M.; Bonalumi, D.; Invernizzi, C.; Iora, P. CO₂ mixtures as innovative working fluid in power cycles applied to solar plants. Techno-economic assessment. *Sol. Energy* **2019**, *181*, 530–544. [[CrossRef](#)]
17. Baik, W.; Lee, W.; Yun, R. Heat transfer and pressure drop characteristics of CO₂ mixtures in a pipeline under the seawater condition. *Int. J. Heat Mass Transf.* **2019**, *136*, 627–634. [[CrossRef](#)]
18. Dai, B.; Li, M.; Ma, Y. Thermodynamic analysis of carbon dioxide blends with low GWP (global warming potential) working fluids-based transcritical Rankine cycles for low-grade heat energy recovery. *Energy* **2014**, *64*, 942–952. [[CrossRef](#)]
19. Yang, M.H. The performance analysis of the transcritical Rankine cycle using carbon dioxide mixtures as the working fluids for waste heat recovery. *Energy Convers. Manag.* **2017**, *151*, 86–97. [[CrossRef](#)]
20. Shu, G.; Yu, Z.; Tian, H.; Liu, P.; Xu, Z. Potential of the transcritical Rankine cycle using CO₂-based binary zeotropic mixtures for engine's waste heat recovery. *Energy Convers. Manag.* **2018**, *174*, 668–685. [[CrossRef](#)]
21. Sun, Z.; Liu, C.; Xu, X.; Li, Q.; Wang, X.; Wang, S.; Chen, X. Comparative carbon and water footprint analysis and optimization of Organic Rankine Cycle. *Appl. Therm. Eng.* **2019**, *158*, 113769. [[CrossRef](#)]
22. Li, X.; Duniam, S.; Gurgenci, H.; Guan, Z.; Veeraragavan, A. Full scale experimental study of a small natural draft dry cooling tower for concentrating solar thermal power plant. *Appl. Energy* **2017**, *193*, 15–27. [[CrossRef](#)]
23. Hu, J.; Liu, C.; Li, Q.; Shi, X. Molecular simulation of thermal energy storage of mixed CO₂/IRMOF-1 nanoparticle nanofluid. *Int. J. Heat Mass Transf.* **2018**, *125*, 1345–1348. [[CrossRef](#)]
24. Chen, X.; Liu, C.; Li, Q.; Wang, X.; Xu, X. Dynamic analysis and control strategies of Organic Rankine Cycle system for waste heat recovery using zeotropic mixture as working fluid. *Energy Convers. Manag.* **2019**, *192*, 321–334. [[CrossRef](#)]
25. Zhou, Y.; Li, Q.; Wang, Q. Energy storage analysis of UIO-66 and water mixed nanofluids: An experimental and theoretical study. *Energies* **2019**, *12*, 2521. [[CrossRef](#)]
26. Usman, M.; Imran, M.; Yang, Y.; Lee, D.H.; Park, B. Thermo-economic comparison of air-cooled and cooling tower based Organic Rankine Cycle (ORC) with R245fa and R1233zde as candidate working fluids for different geographical climate conditions. *Energy* **2017**, *123*, 353–366. [[CrossRef](#)]
27. Hooman, K. Dry cooling towers as condensers for geothermal power plants. *Int. Commun. Heat Mass* **2010**, *37*, 1215–1220. [[CrossRef](#)]
28. NIST Webbook. Available online: <http://webbook.nist.gov/chemistry/fluid/> (accessed on 1 June 2019).
29. Lemmon, E.W.; Huber, M.L.; McLinden, M.O. *NIST Standard Reference Database 23: Reference Fluid Thermodynamic and Transport Properties Refprop*; Version 9.1; NIST: Gaithersburg, MD, USA, 2007.

30. Pioro, I.L.; Khartabil, H.F.; Duffey, R.B. Heat transfer to supercritical fluids flowing in channels—Empirical correlations (survey). *Nucl. Eng. Des.* **2004**, *230*, 69–91. [[CrossRef](#)]
31. Petukhov, B.S. Heat Transfer and Friction in Turbulent Pipe Flow with Variable Physical Properties. In *Advances in Heat Transfer*; Hartnett, J.P., Irvine, T.F., Eds.; Elsevier: Amsterdam, The Netherlands, 1970; pp. 503–564.
32. Cengel, Y.A.; Klein, S.; Beckman, W. *Heat Transfer: A Practical Approach*; McGraw-Hill: New York, NY, USA, 1998; Volume 141.
33. Kröger, D.G. *Air-Cooled Heat Exchangers and Cooling Towers*; PennWell Books: Tulsa, OK, USA, 2004; Volume 1.



© 2019 by the authors. Licensee MDPI, Basel, Switzerland. This article is an open access article distributed under the terms and conditions of the Creative Commons Attribution (CC BY) license (<http://creativecommons.org/licenses/by/4.0/>).